International Journal of Material Forming (2019) 12:761–776
https://doi.org/10.1007/s12289-018-1446-z

ORIGINAL RESEARCH

Enabling sheet hydroforming to produce smaller radii on aerospace nickel alloys

Colin Bell[1] · Caleb Dixon[2] · Bob Blood[2] · Jonathan Corney[1] · David Savings[3] · Ellen Jump[4] · Nicola Zuelli[4]

Received: 25 April 2018 / Accepted: 25 September 2018 / Published online: 18 October 2018

Abstract

This paper presents the first academic study of a hydroforming process known as edging. An edging process allows a smaller radius to be produced with a lower pressure than a standard sheet hydroforming process and is currently developed by trial and error that relies heavily on operator experience. This paper reports the first systematic investigation of the edging process that concludes in a new analytical model which can be used to enable the design of edging processes. It was found that in each of the three aerospace nickel alloys tested, the edging technique was effective in sharpening the flange radius from 10 mm to 4 mm or from 6 mm to 2 mm in thicknesses of 2.1 mm and 1.2 mm respectively. This radius is equivalent to between 1.5 and 1.8 times the material thickness (1.5 t to 1.8 t). These results were achieved by using edging heights of between 2.5 to 5 mm (2.5 t to 3 t). At the limits of successful edging operations, (under 2 t) three different kinds of phenomena were observed: crushing of the top of the component, radii which were pushed inwards, and the generation of an underside lip which protruded from the bottom of the samples. This paper discusses the benefits of hydroforming with an edging operation, explores the limitations of the edging process, derives an equation which can be used to estimate the sharpness of an edged radius and finally defines a model which enables the design of an edging operation. The work reported here is particularly relevant to aerospace applications because it will enable lighter components to be formed with lower pressures with nickel based superalloys.

Keywords Hydroforming · Fluidforming · Cold forming · Near-net-shape manufacturing · Forming · Edging

Introduction

Hydroforming is a well-established near net shape manufacturing process that is currently used in many industries, including the automotive [1] and aerospace [2] industries, to form complicated geometries from metal blanks. Hydroforming works by using fluid pressure in conjunction with mechanical forces to form metal tubular and sheet components. The utilization of evenly distributed fluid pressure results in several key process advantages such as deeper draw depths, more accurate feature generation, and excellent surface quality [3]. While there are many refinements to the basic hydroforming technique that can be used to achieve a specific geometry [4], this paper investigates a process enhancement known as edging. In this process, the punch is extended higher than the required draw depth and then lowered back down a few millimeters while the fluid pressure is increased. This has the effect of tightening the radius between the flange and the drawn portion of the component beyond the values achievable in a normal sheet hydroforming operation. This is important in sheet hydroforming operations because often the limitation is the smallest radius. In fact, the pressure required for an operation is almost entirely dependent upon the material properties, the thickness, and the smallest radius of the formed component. [5] Consequently, having an alternate technique to sharpen a radius (other than increasing fluid pressure or using thinner material) expands the capability of the process.

Figure 1 illustrates how edging is implemented in a sheet hydroforming operation; first a blank is first lubricated and positioned on top of the draw ring and punch (Fig. 1a). The fluid is then pumped in from above and fills a rubber bladder

✉ Colin Bell
Colin.Bell@strath.ac.uk

[1] Design, Manufacture and Engineering Management, University of Strathclyde, 75 Montrose St, Glasgow G1 1XJ, UK

[2] Triform, 889 Horan Dr, Fenton, MO 63026, USA

[3] Rolls-Royce plc, PO Box 31, Derby DE24 8BJ, UK

[4] Advanced Forming Research Centre, 85 Inchinnan Drive, Inchinnan, Renfrewshire PA4 9LJ, UK

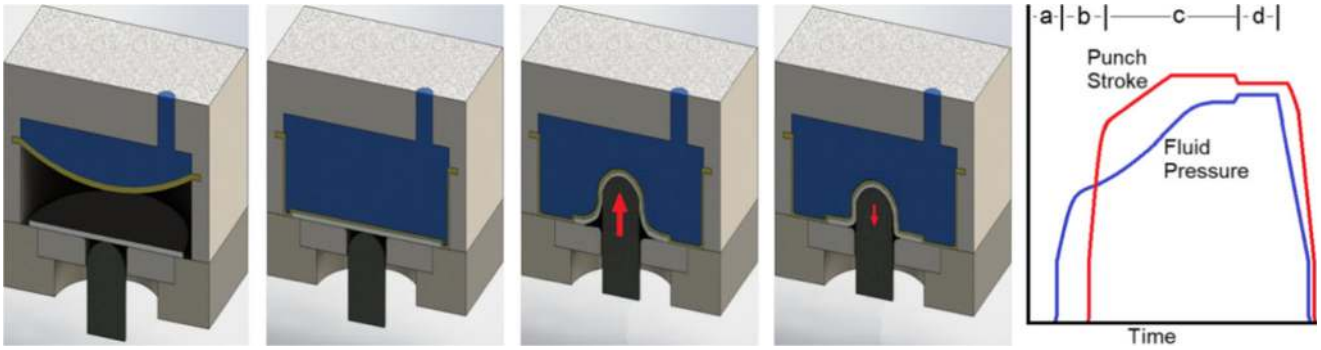

a) Blank placed on draw ring, press sealed | b) Chamber filled with fluid | c) Punch engaged, fluid pressure increased | d) Edging - punch retracted with slight pressure increase | e) Representative stroke and pressure

Fig. 1 Hydroforming with edging schematic

expanding it downwards (Fig. 1b). The fluid pressure is increased until the chamber fills completely and the bladder is firmly pressed against the blank (Fig. 1c). Then the punch is engaged and starts travelling upward as the fluid pressure continues to increase. The high fluid pressure, forces the blank tightly against the punch which forces the blank to conform precisely to the shape of the punch. The goal of the pressure cycle is to create conditions where the fluid pressure is high enough to prevent wrinkling and low enough to allow material to be drawn into the working zone from the flange (which helps avoid thinning and tearing). Towards the end of the pressure cycle, the edging process starts when the punch is retracted and the fluid pressure increased a small amount further. This drop of the punch has the effect of allowing material to flow into the radius from the previously formed dome as well as the flange. In this study we consider a domed geometry for demonstration of the edging process which starts as a 127 mm diameter blank and forms into a half spherical domed geometry through the sheet hydroforming process. This can be seen schematically alongside a representative pressure cycle in Fig. 1e.

The generic structure of hydroforming equipment includes the fluid, rubber bladder, draw ring and punch which are illustrated in Fig. 2 alongside the different points of interest on the formed samples. Of particular importance in this work is the flange radius (r_1) which is measured and studied during the results section.

Hydroforming is a complicated process as the sample is not constrained mechanically by draw beads or a blank holder and for this reason there can be several deformation mechanisms. As the process begins, the sample undergoes bending as the punch pushes the middle of the sample up while the sample is constrained around the edges by fluid pressure. The authors hypothesize that the sample is then stretched with the primary strain in tension and minor strain in compression similar to those seen in a deep drawing operation (highlighted in Fig. 3). It is also likely that the flange undergoes localized compression, as other works which have analyzed the same geometry have reported thickening in the edge of the flange and compressive minor strain rates [8].

Aim and objectives

The aim of this investigation is to reduce the time taken to develop edging operations. This aim will be delivered by the following objectives:

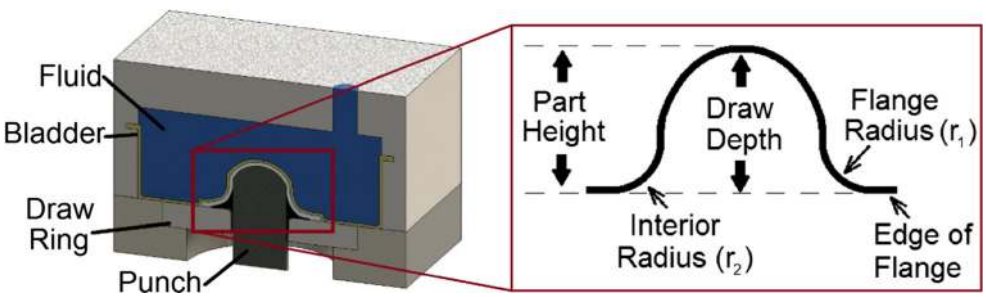

Fig. 2 Terminology of hydroforming equipment and generic formed part

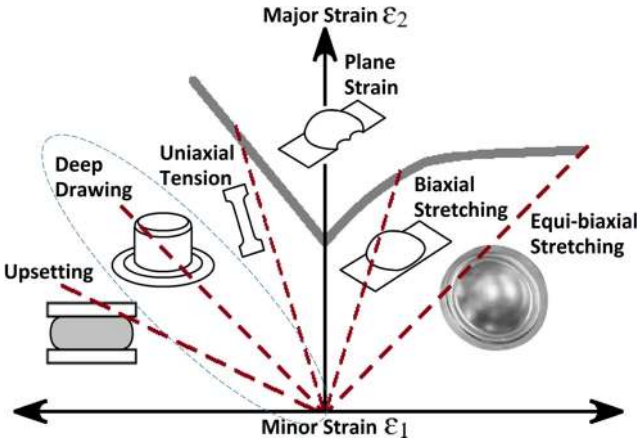

Fig. 3 FLD with likely applicable strain condition circled; redrawn from [6, 7]

1) Investigation of the relation between edging parameters and formed component geometry
2) Derivation of an analytical model of the edging process
3) Determination of the model's forming coefficients based upon trial results
4) Discussion of the model's accuracy and limitations

The rest of this paper is structured as follows. The following section describes the rationale for the materials used in the experiments. Then the tensile testing method used to gather mechanical properties is discussed with the results presented. A literature section follows which briefly outlines the relevant academic literature, then an analytical model of the edging process is proposed. The subsequent section reports how the model's application has been assessed experimentally and then the results are discussed and conclusions drawn.

Material properties

Nickel alloys are durable materials well known for their capacity to operate sustainably at extremely high temperatures for extended periods of time. This combination of properties makes them ideal candidates for aerospace applications, particularly in gas turbine engines where operating temperatures can be in excess of 600 °C. Although strong, nickel alloys are also reasonably ductile and consequentially can be formed by a number of different processes, albeit with higher pressures than are required with other metals. Figure 4 illustrates the relative forgeability, (i.e. the ability of a material to be taken from a blank shape and formed into a final shape) relative to the forces required to do so.

There are many nickel alloy components currently used in gas turbine engines which require the flange as an integral part of the final geometry (i.e. the flange is not removed after forming). Since weight and physical space is at a premium in aerospace applications, having a component geometry with

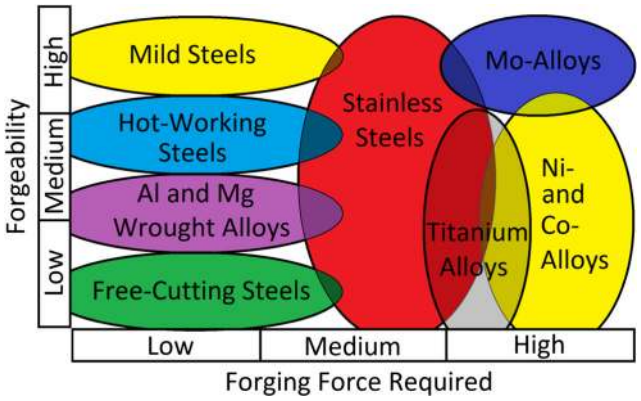

Fig. 4 Forging forces versus forgeability for various metals; redrawn & translated from [9]

a smaller flange radius is beneficial as it can free up space in the vicinity of the component and allow for a more compact design. Consequently the investigation of the edging process reported here is motivated by the potential opportunity for more compact designs and lower manufacturing costs in aerospace applications [2].

Three nickel alloys were examined in this study: Nimonic C263 (2.07 mm thickness), Inconel 718 (1.23 mm thickness), and Nimonic 75 (1.23 mm thickness). The chemical compositions of these alloys can be seen in Table 1.

Sheet tensile testing

Tensile tests were carried out to determine mechanical properties such as yield strength (0.2% proof stress), ultimate

Table 1 Representative chemical compositions of C263, Inconel 718, Nimonic 75 (wt%) [10–12]

Composition	Inconel 718	Nimonic 75	Nimonic C263
Nickel	50 - 55	Balance	Balance
Cr	17 - 21	18 - 21	19 - 21
Fe	Balance	5.0 (max)	0 - 0.7
Nb	4.75 - 5.5		
Mo	2.8 - 3.3		5.6 - 6.1
Ti	0.64 - 1.15	0.2 - 0.6	1.9 - 2.4
Al	0.2 - 0.8		0.3 - 0.6
Co	1 (max)		19 - 21
C	.08 (max)	.08-.015	0.01 - 0.08
Mn	.35 (max)	1.0 (max)	0 - 0.6
Si	.35 (max)	1.0 (max)	0 - 0.4
P	.015 (max)		0 - 0.015
S	.015 (max)		0 - 2.4
B	.006 (max)		0 - 0.005
Cu	0.3 (max)	0.5 (max)	0.2 (max)

tensile strength (UTS), and the modulus of elasticity (MOE) of each material. Samples were cut at 0, 45 and 90 degrees to the rolling direction, using electrical discharge machining (EDM) as seen in Fig. 5. While it was assumed that there would be no strain rate sensitivity at room temperature, three different strain rates were tested on the samples to confirm this. Strain rates of 0.01, 0.1 and 0.5 s^{-1} were used. With each round of tensile testing the procedure entailed first testing an extra sample (which had been cut at 45 degrees) to calibrate the test and ensure proper setup, and then one sample in each direction was tested at each strain rate.

Limited material was available for these tests, and so it was not possible to use the standard sheet tensile sample size as specified ASTM E8 and instead an alternate geometry which follows the same principles and has been used industrially in the past was chosen. Dimensions of the tensile specimen are detailed in Fig. 6.

Tests were performed at room temperature as it has been assumed that there is minimal heat generation during the hydroforming process. Testing was performed on a Zwick/Roell Z150 tensile testing machine, to ISO-6892 standard. Full test results cannot be published in this work for reasons of commercial sensitivity, however flow stress curves were generated using Zwick proprietary software and the elongation and strain hardening behavior of each alloy was examined. The material yield point at which plastic deformation begins is of particular interest to this work and this was calculated for each sample using the 0.2% offset method, whereby a line is constructed parallel to the initial linear portion of the stress strain curve, offset from the origin by 0.002 strain (0.2%). The point at which this line intersects the stress strain curve for each tensile sample was taken as the yield point, and the results for each material (across all strain rates and rolling directions) were averaged to find a value for each alloy (shown in Table 2).

Table 2 Average mechanical properties of tensile results

Material	Proof stress (MPa)
Inconel 718	450.05
Nimonic 75	482.44
Nimonic C263	385.30

The effect of the strain rate was examined by comparing the stress-strain curves of each of the three strain rates tested (0.01, 0.1, and 0.5 s^{-1}) and found to be negligible at room temperature as can be seen in Fig. 7 as the stress-strain curves all coincide closely. Due to the small specimen size it was not possible to use an extensometer to determine the r value (plastic anisotropy ratio), but the anisotropy can be seen visually in Fig. 8 where there is a noticeable difference between the stress-strain curves of different orientations to the rolling direction. The sample in the rolling direction (0 RD) shows the largest strain hardening. Strain hardening is a phenomena wherein a material undergoing plastic deformation becomes stronger and is most noticeable with the 0 RD samples. This is displayed by the increased amount of strain required to induce deformation (i.e. the 0 RD curve is higher than the other curves). This is important to hydroforming because during the process the material deforms plastically and

Fig. 5 Tensile Samples cut from blanks showing orientation

b	Lo	Lc (min)	r	Lt	W
Gauge Width	Gauge length	Parallel length	Transition radius	Total length	Total Width
3 ± 0.03	25	27	6	52	9.5

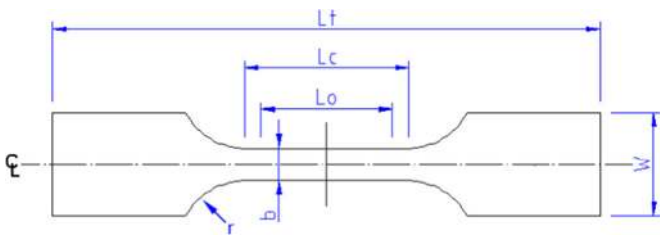

Fig. 6 Dimensions of the tensile testing specimens (mm)

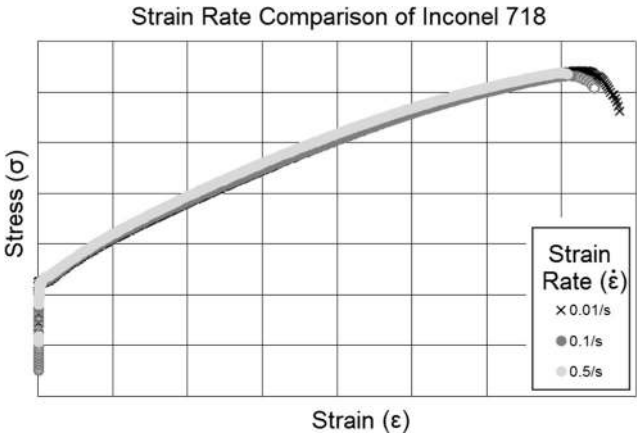

Fig. 7 Strain rate comparison of Inconel 718

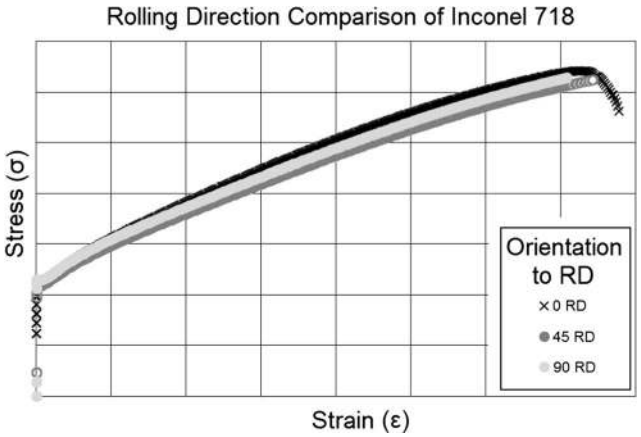

Fig. 8 Mechanical properties by orientation of Inconel 718 (at $\dot{\varepsilon} = .01$)

because of the variation in the cold rolled material depending upon rolling direction, the material will deform anisotropically.

Literature survey

Many scientific studies have been published regarding the flange and flange radius as they relate to hydroforming operations. For example, Nakamura et al., state that for parts with a smaller radius the "liquid pressure press-forming method requires partial use of coining dies or restriking in the subsequent process." [13] This secondary operation which is used to sharpen radii is known in the hydroforming industry as coining. While the term coining normally refers to a closed die forming operation in which all surfaces are restrained resulting in an imprint of the die on the work piece, in this instance coining refers to a "restriking operation used to sharpen or change an existing radius or profile" [14]. In tube hydroforming operations, a similar effect (also called coining) exists in where a radius inside a certain feature, such as a T branch, is sharpened. In one such study of tube hydroforming published by Crapps et al., the pressure was increased from roughly 35 to 75 MPa at the end of the T branch creation in a coining stage. This increased pressure ensured that the final radii of the newly created T branch matched the die [15]. Ceretti et al., looked into a tube hydroforming operation in which the objective of creating vases was inhibited in part by the complicated geometry including the fillet radii [16].

Danckert and Nielsen looked at modifying a hydromechanical deep drawing process to apply a uniform pressure to the flange and achieved a draw ratio of as high as 3.0 with aluminum cups [17]. Others such as Wang et al., have used radial pressure to assist in the inwards flow of the flange and showed that could increase draw ratios from 2.5 to 2.8 [18]. Shang et al., performed a hydroforming operation in which they allowed "draw-in" for one stage (in a two stage hydroforming process) but not in the second stage. This resulted in an increase in formability [19]. But while they suggest sharpening the shoulder radius aids formability, it was not stated whether a two stage process aids in producing geometries with sharper radii.

The techniques described in the literature are similar to edging in that they either impact the flange draw in, or the final formed radius, but none of them do so by retracting the punch. Edging shows a clear benefit over coining in a secondary restriking operation as it allows for the creation of the sharper radius in a single cycle operation. Additionally, as compared to the use of a much higher fluid pressure to create a sharper radius at the end of a forming cycle, edging has an advantage in that it can be carried out on lower capacity equipment with a quicker manufacturing time.

There have been many other recent strands of hydroforming research but these have mostly explored new technological developments based upon new hydroforming processes and consequently did not directly investigate flange radius generation. For example the subject of hot hydroforming is a topic of active research with recent works such as Aissa et al. who reported findings on a hydroforming using steam as a forming medium on aluminum sheet metal [20], or Yuan et al. [21] who used hot oil to form an AZ31 magnesium alloy tube or Landgrebe & Schieck who published a work using hot gas hydroforming [22]. Ruez & Knoll published a work on a new hybrid process for tube hydroforming and injection molding which can be used in automotive applications. Other works included Liu et al. who looked at implementing a pre-bulging stage during a hydroforming process to increase formability [23], Bach et al. looked at impulsive forming of tubes through gas detonation [24], Rösel & Merklein and later Wang et al. looked into using smart fluid in a hydroforming operation which could change viscosity by using electromagnetism [25, 26]. While all of these areas of research are actively advancing hydroforming technology, none of them mention the generation of the flange radius and are therefore outside the scope of this work.

Theory

A mathematical model can be derived which relates a final value for an edging radius based upon an initial radius and an edging height. This is done by considering the dimensions of a non-edged component (shown in black) and an edged component (shown in grey) in Fig. 9. The geometry is simplified by only considering the outside edge and not the entire thickness. The outside edge is chosen because this is where the radius is measured and is typically the significant aspect in industrial applications. By defining a control volume for the geometry around the larger radii, the length of the new and old geometry inside the control volume can be calculated (Eqs. 1 & 2). In the following: r_{1a} is defined as the flange radius before edging, r_{1b} is the flange radius after edging, and b_x is the linear portion of the edged radius which has been straightened through the edging process.

Now consider that the edging operation lowers the punch a certain distance to create additional material which will be pushed into the corner. This edging height (W) is set manually by programming in a value based upon operator experience. By controlling the edging height, more or less material can be made available to tighten the radius. The edging height is therefore directly proportional to the difference between the length of a and the length of b. This proportional relationship can be characterized by assuming that the difference between the new length and the old length is equal to W multiplied by a loss coefficient k (Eq. 3). There is also a geometric relationship between the two radii (i.e. old and new) and the linear portion they are associated with (Eq. 4). All 4 of these equations and the variables are defined below in Fig. 9.

Substituting Eqs. 1 and 2 into Eq. 3 yields:

$$\left(\frac{1}{4}\right)*2\pi r_{1b} + 2b_x - \left(\frac{1}{4}\right)*2\pi r_{1a} = k*W$$

Substituting the expression for b_x in Eq. 4 yields:

$$\left(\frac{1}{4}\right)*2\pi r_{1b} + 2(r_{1a} - r_{1b}) - \left(\frac{1}{4}\right)*2\pi r_{1a} = k*W$$

Simplifying the resulting equation with a numerical approximation for pi, and solving for r_{1b} (the radius that the edging operation will produce) yields:

$$r_{1b} = r_{1a} - \frac{k*W}{0.43} \tag{5}$$

In Eq. 5, the value W is specified by the operator as part of the process, the value for k is an empirical value determined experimentally, and the value for r_{1a} will be measured with a baseline sample for which the hydroforming process will not include an edging operation. Taking this one step further, the literature suggests an equation which is used to estimate a radius based upon yield strength (YS) and fluid pressure given by Koç [5]:

$$Fluid\ Pressure = \frac{YS*t}{r} \quad \text{Solving for r yields :} \quad r = \frac{YS*t}{Fluid\ Pressure} \tag{6}$$

Substituting Eq. 6 into the value for r_{1a} in Eq. 5 yields Eq. 7. Alternatively the equation can be solved for W which would be useful if a radius was set and a required edging height was desired as shown in Eq. 8.

$$r_{1b} = \frac{YS*t}{Fluid\ Pressure} - \frac{k*W}{0.43} \tag{7}$$

$$W = \frac{0.43}{k}*\left(\frac{YS*t}{Fluid\ pressure} - r_{1b}\right) \tag{8}$$

So with a forming pressure and an edging height that are set on the press, as well as a yield strength, a thickness, and the constant k, an approximation of a radius in a hydroforming process with an edging operation can be estimated. However it should be noted that the equation given by Koç [5] is only able to give an approximate value of the required forming pressure for a hydroforming operation. In the next section a series of experiments is reported that assesses the proposed relationship between the variables in the edging model.

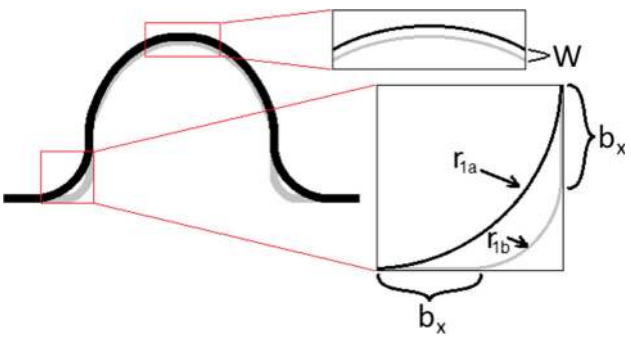

$$Length_a = \left(\frac{1}{4}\right)*2\pi r_{1a} \tag{1}$$

$$Length_b = \left(\frac{1}{4}\right)*2\pi r_{1b} + 2b_x \tag{2}$$

$$Length_b - Length_a = k*W \tag{3}$$

$$r_{1a} - r_{1b} = b_x \tag{4}$$

Fig. 9 Theoretical geometry & geometric equations

Experimental setup, materials and blank geometry

A series of edging trials were conducted on a Triform sheet hydroforming press model 610–20-3SC with deep draw capability which had a 138 MPa (20,000 psi) fluid pressure capability and a bladder separating the workpiece from the acting fluid.

Three different materials were selected for the trials on the basis of their potential for use in aerospace engine applications. As per the specification of the tooling, all of the sheets were laser cut into 127 mm diameter blanks and numbered with the rolling direction indicated on the surface. The blank size was set by the existence of tooling already in use for experimental purposes at the manufacturer's facility (Beckwood Presses) which had a punch with a 65 mm diameter, a draw ring, and a gap of 0.75 mm between the punch and ring as shown schematically below in Fig. 10. The machine interface operates with traditional units (inches, psi etc...) which have all been converted to SI for the purposes of this paper.

Six samples of three different grades of nickel were tested during the experiments. The three materials used were Nimonic C263 aerospace grade nickel with a thickness of 2.07 mm, 1.23 mm thick Inconel 718, and 1.23 mm thick Nimonic 75.

Experimental procedure

The objectives of the trials were:

1. Find the largest draw possible for each material using the 127 mm diameter blank. This is done by stopping the first few experiments several times to visually examine how the hydroforming operation is proceeding and adjusting the parameters accordingly.
2. Find the limits of the edging operation observing what happens when these boundaries are exceeded, and determine the minimum radius achievable between the flange and the drawn portion for each grade of nickel.

The trial plan followed an iterative approach using the first few blanks to search for the largest draw depth that could be successfully achieved. Standard parameters were first chosen by the supplier based upon experience and these were altered slightly with the first few samples until a successful draw depth and part formation was achieved. This was used as the baseline (control) sample. Then the rest of the samples were formed following the exact same pressure cycle, but with an incrementally increasing edging operation at the end to see when failure or abnormalities occurred. A user interface for the machine as well as the various stopping points for the initial trial are shown below in Fig. 11.

Edging behavior at the forming limit

There were three distinct kinds of behaviors that were observed to occur with large edging operations which are shown in Fig. 12. The first was crushing the upper portion of the sample's dome. In applications where the flange and radius are important and the top section was to be removed, like those tested by Mohammed et al. [27], the crushing could be inconsequential to the final product. The second kind occurred when the radius became too sharp, and the material bent too far downwards which caused a negative radius (the value for r_1 was reduced past 0 and subsequently bent inwards). Unless the flange was going to be removed entirely, this would significantly weaken the strength of the component in the transition area between the flange and drawn portion. The third was the bulging of the material downwards into the gap between the punch and draw ring. If this third kind was mild enough (like the kind discussed later in Fig. 16) it could possibly be turned or ground off after the process or there may be a few situations in which it is beneficial (e.g. location in an adjacent part, or for a seal around a gasket). Furthermore if the inside radius was critical, then in certain circumstances it is beneficial to generate an underside lip and turn down the product to get a sharper inside radius with a machined tolerance.

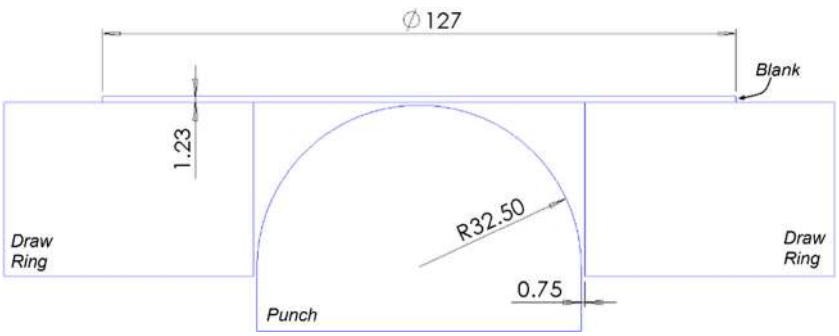

Fig. 10 Dimensions of sheet hydroforming test rig

STEP	PUNCH POSITION (INCHES)	BLADDER PRESSURE (PSI)	DWELL TIME (SECONDS)	OPEN PRESS
1	0.000	1000.0	0	OPEN OFF
2	0.100	1300.0	0	OPEN OFF
3	0.250	2000.0	0	OPEN OFF
4	0.400	3000.0	0	OPEN ON
5	0.600	6000.0	0	OPEN OFF
6	0.700	7500.0	0	OPEN OFF
7	0.875	8000.0	0	OPEN ON
8	1.000	8500.0	0	OPEN OFF
9	1.150	9500.0	0	OPEN OFF
10	1.300	11000.	0	OPEN ON
11	1.700	11250.	0	OPEN OFF
12	1.600	11500.	2	OPEN OFF
13	0.000	0.000	0	OPEN OFF
14	0.000	0.000	0	OPEN OFF
15	0.000	0.000	0	OPEN OFF

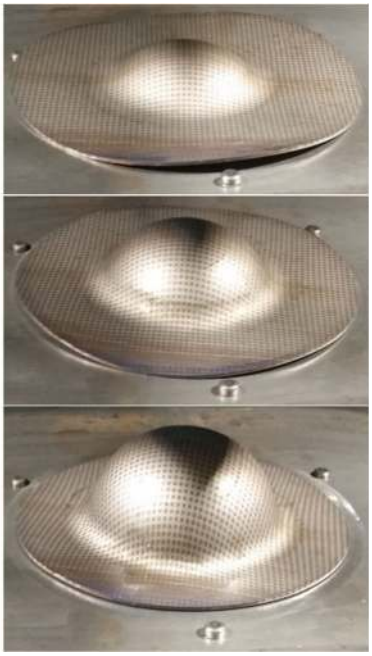

Fig. 11 Representative forming parameters and sample geometry. Pictures taken at "Open On" Positions

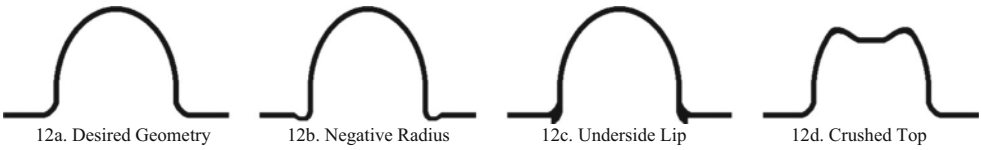

Fig. 12 Hydroforming abnormalities generated at the limits of the edging process

Results

The tightest flange radius without any of the abnormalities seen in Fig. 12 results for the 2.07 mm thick C263 alloy sheet were achieved with a 33 mm draw depth and a 5.08 mm edging operation (i.e. punch withdrawal) which produced an average radius of 3.5 mm as opposed to 10 mm in the baseline sample without edging. Fig. 13 shows the baseline sample while Fig. 14 shows the much tighter radius achieved with edging. When a larger edging operation of 6.35 mm was attempted, the same radius of 3.5 mm was achieved, and the additional 1.27 mm edging distance appeared to be absorbed (at least in part) by slightly crushing the top of the dome as seen in Fig. 15 (schematically represented in Fig. 12d). When an even larger edging operation of 8.9 mm was attempted, the flange radius was not improved and the top of the dome crushed even more significantly and an underside lip was formed as can be seen in Fig. 16 (or schematically in Fig. 12c). Therefore even in cases when the top of the dome is to be removed after the forming operation, it would not necessarily help to perform a large edging operation which crushes the dome as the results were, if anything, counterproductive with respect to sharpening the radius. In specific cases where a smaller radius must be achieved, it would likely be best to consider coining to set the radius instead of (or in conjunction with) edging.

Building upon the results of the first trial, the hydroforming process parameters for the second trial were mostly carried over, except for a slightly higher pressure in the middle stages to increase the force on the flange to prevent excessive early material draw in from the flange (discussed later in Fig. 24). The best results for the 1.232 mm thick Inconel 718 alloy were achieved with a 43.2 mm draw depth and a 3.81 mm edging operation which produced an average flange radius of 2.25 mm. This result along with the baseline sample can be seen below in Figs. 17 and 18. A higher draw depth of 5.08 mm yielded a very slight negative radius

Fig. 13 Baseline C263 without edging

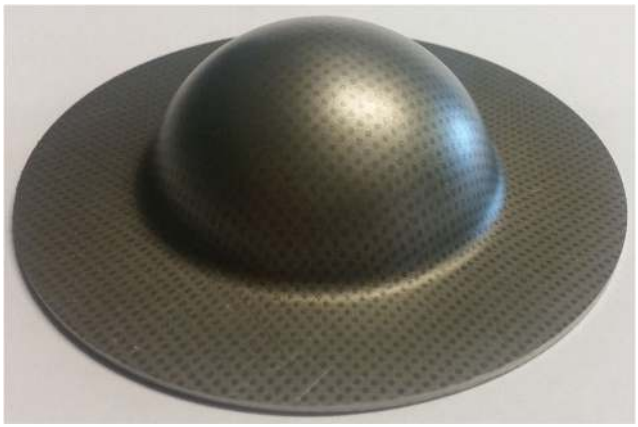

Fig. 14 5.08 mm successfully edged C263

Fig. 15 6.35 mm edged C263 with a slightly crushed top

(see Fig. 12b) and underside lip in one small location as can be seen in Fig. 19.

The results for the 1.232 mm thick Nimonic 75 alloy were almost identical to the results of the Inconel 718 trials. The largest edging operation without abnormalities was achieved with a 43 mm draw and a 3.81 mm edging operation which produced an average flange radius (r_1) of 1.875 mm. The baseline result can be seen in Fig. 20 with the edged result in Fig. 21 for comparisson. The 5.08 mm edging operation produced a much more pronounced negative radius and underside lip as compared to the similar trial in Inconel 718 as can be seen in Fig. 22.

All of the radii were measured with a set of incremental radius gauges which measured in 0.25 mm increments for small radii between 0 and 4 mm and 0.5 mm increments between 4 and 7 mm (the accuracy of these gauge measurements is later checked using optical microscopy). The measurements were taken at 4 places around the circumference. At measurement locations 1 and 3 the measured radius was orthogonal to the rolling direction, and at measurement locations 2 and 4 the radius measurement was parallel to the rolling direction. The measurement locations can be seen below Fig. 23.

In Table 3, the trials are listed chronologically. The thicker C263 samples were tested first, followed by the Inconel 718 and then the Nimonic 75 samples. The thickness of the C263 samples meant that the limit of the available punch force was reached at a draw of 33 mm. Therefore a part height of 33 mm was chosen for the C263 experiments. After the baseline model was set, 3.175 mm and 5.08 mm edging operations were attempted with success. 6.35, & 8.9 mm edging operations were then attempted which resulted in signs of top crushing and an underside lip. The smallest radius that was achieved on the C263 material was 3.5 mm as compared to the 10 mm baseline sample.

As mentioned above, the results for the Inconel 718 and Nimonic 75 trials were similar, with the main difference being the abnormalities present in the 5 mm edging height. The Nimonic 75 had a more pronounced underside lip and an entirely circumferential negative radius. This means that the Inconel 718 sample could have likely been edged a bit further, to a value between 4 and 5 mm and the radii tightened a little more without the appearance of abnormalities.

To make results more widely applicable, values were normalized by dividing by material thickness. This ratio of radius/thickness (r/t) allows for test results to be applied to a much wider range of sheet metal sizes and for direct comparison between parts of different thicknesses. The results of this set of experiments therefore showed that the r/t ratio can be reduced from around 5 t without edging to a value of around 1.5 t - 2.0 t with edging. Values tighter than this lead to the formation of negative radii, crushed tops, and underside lips. The full results can be seen below in Table 3 (note: all radius values reported are flange radius values, r_1).

Using Eq. 5 (which uses the baseline sample for r_{1a}) we can estimate a value of k by computationally minimizing the error produced in the samples. Ignoring samples with abnormalities and minimizing the absolute error of the edging samples

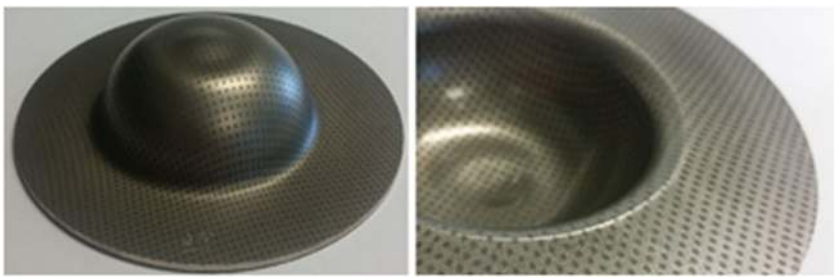

Fig. 16 8.9 mm Over-edged C263 with a crushed top and underside lip

Fig. 17 Baseline Inconel 718

yields a k value of 0.55 and an average error of 13% (σ = 10%). One significant observation is that the calculated radius and r/t values get extremely small (and sometimes negative) with a large edging operation. Therefore Eq. 5 appears to be accurate as long as the calculated r/t value is above 2. The error of the calculated radius values from Eq. 5 as opposed to the measured values from the trials can be seen in Table 4.

Running a test to measure a value for r_{1a} on a hydroformed component without edging, and then using Eq. 5 is more accurate than estimating with Eq. 7. The equation from the literature (Eq. 6) which estimates a radius is compared with the measured radius values below in Table 5. Since Eq. 6 is used in the derivation of Eq. 7, the error shown below would translate into additional errors in the radius calculation when using Eqs. 7 or 8. Even when re-optimizing the k value, the error increases from an average error in Eq. 5 of 13% to an average error in Eq. 7 of 20%. For this reason, Eq. 5 was used in the calculations for this set of trials.

Optimized forming and edging process parameters

The parameters associated with successful forming operations achieved with each alloy are summarized in Fig. 24. These represent the maximum edging operations that were achieved without the development of the aforementioned abnormalities.

Effect of edging on overall part height

A separate result from this experiment was the observation that a certain value given for an edging operation does not necessarily lead to an identical value for the drop in part height in the final component. For example when a 3.175 mm edging operation was performed on the 2.07 mm thick Nimonic C263, the part height decreased 2.21 mm which is about 30% less than would be expected. This could be caused by a variety of factors including material thinning, springback, and backlash (mechanical play/losses) in the press. While there was a strong correlation between the edging height and the part height change, the values were not identical and differed by 10 to 30% of the edging height. This means

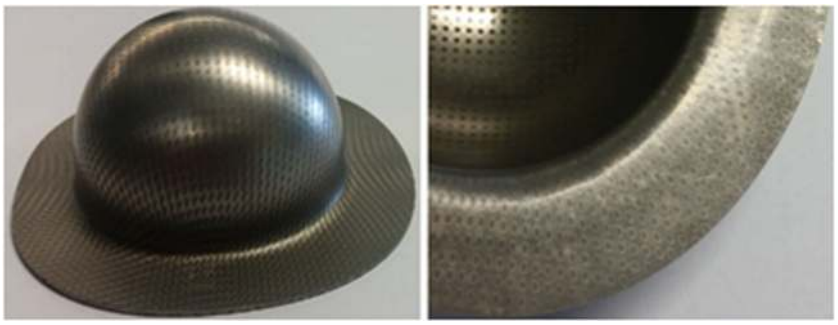

Fig. 18 3.81 mm successfully edged Inconel 718

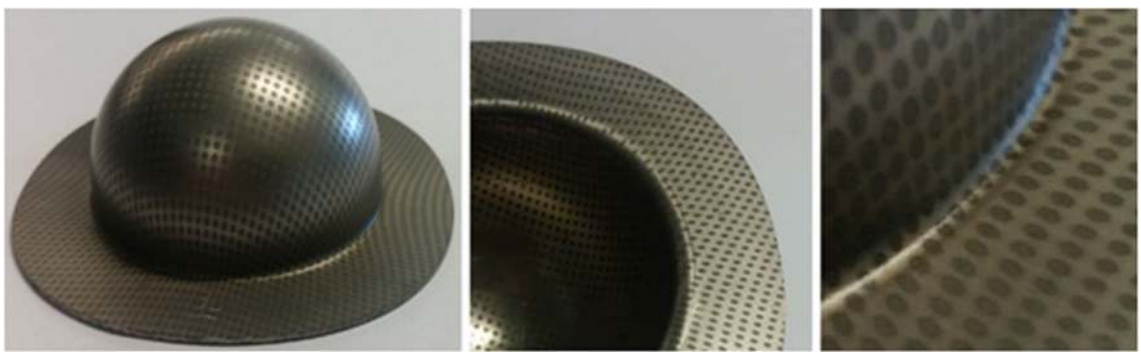

Fig. 19 5.08 mm slightly over-edged Inconel 718 with an underside lip and a small negative radius in 1 location

Fig. 20 Baseline Nimonic 75

that (for example) if an edging height of 5 mm was used, the part will be roughly 4 mm shorter (20%).

The edging operations lowered part height between 10 and 30% less than the edging height (punch withdrawal distance) as compared to the non-edged samples. This would mean that from a design perspective, an additional 10 to 30% of the edging height should be added to the draw depth to compensate for non-linear effects and properly estimate final part height.

The experimental results, equations, and observations can be synthesized into a procedure for designing for hydroforming with an edging operation (Fig. 25). This process should allow an engineer to define a procedure which generates results close to the final geometry they desire. However trials or finite element analysis (FEA) simulations should also be used when tolerances are tight.

Sheet thickness and radius measurement

To measure the sheet thickness and verify the accuracy of the previous radius measurements (made by radius gauges) each set of materials was water jet cut into quarters and measured via optical microscopy. The same sample set as defined above i.e. those formed by the optimized forming and edging parameters, was chosen. First the samples were water-jet cut and temporarily mounted on their side. Then a 2D surface profile was examined with an Alicona infinite focus G4 with a magnification of 2.5× which had facility for 2D thickness and radius measurements of the surface profile. An example of a sample marked for cutting and the resulting quarter section can be seen in Fig. 26 (alongside the schematic of the measurement locations).

After cutting, the following dimensions were measured: flange radius (r_1), larger interior radius of the dome (r_2), and material thickness in the middle of the radius. Examples of this measurement technique are shown in Figs. 27 and 28 (terminology was covered in Fig. 4).

The values obtained using this technique were compared to the previous radius measurements (Table 3) and were found to be in general agreement showing an average absolute difference of 5.25% ($\sigma = 6.35\%$) as shown in Tables 6 and 7. This confirms the accuracy of the radius gauge measurement

Fig. 21 3.81 mm successfully edged Nimonic 75

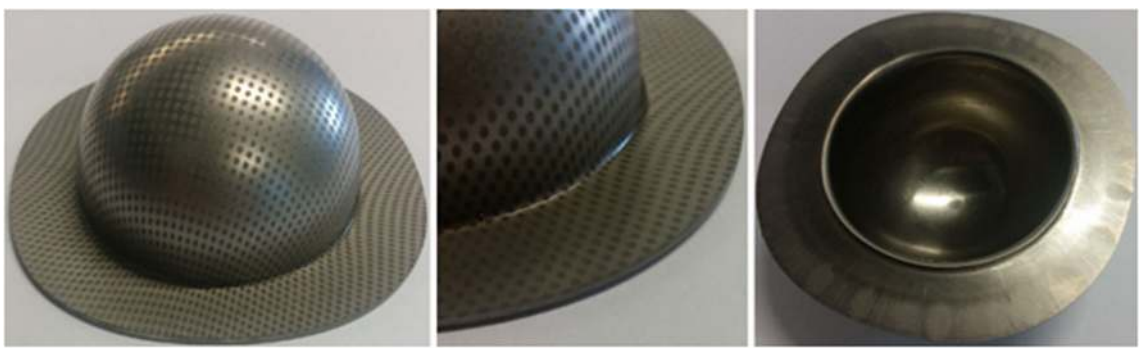

Fig. 22 5.08 mm over-edged Nimonic 75 with a negative radius and pronounced underside lip

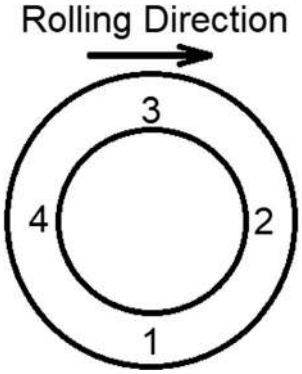

Fig. 23 Location of radii measurements with respect to rolling direction

method and the validity of the governing equations that were based upon these measurements.

Counterintuitively, the material in all cases did not thin at the radius and in fact thickened by between 6 and 21%. The authors speculate that this might be caused either by the edging operation pushing material into the radius section causing thickening, or possibly the drawing action pulling in more material from the flange and forcing it to conform to a smaller diameter. The thickness was measured independently (instead of subtracting the two radius measurements) to ensure a more accurate measurement which is important in cases where the radius is variable and oblong (and not homogenous).

Table 3 Table of experimental results

Material	Mat'l Thickness (mm)	r1 (mm)	r2 (mm)	r3 (mm)	r4 (mm)	Ave r (mm)	Edging Height (mm)	r/t	Result
C263	2.07	10	10	10	10	10.0		4.8	33 mm Baseline Draw
C263	2.07	6	5.5	5.5	5.5	5.63	3.175	2.7	Success
C263	2.07	3.5	3.5	3.5	3.5	3.50	5.08	1.7	Success
C263	2.07	3.5	3.5	3.5	3.5	3.50	6.35	1.7	Top Crushed Slightly
C263	2.07	4	3.5	3.5	4	3.75	8.89	1.8	Top Crushed, Underside Lip
Inco 718	1.23	7	7	6.5	7	6.88		5.6	43 mm Baseline Draw
Inco 718	1.23	3	3	3	3	3.00	2.54	2.4	Success
Inco 718	1.23	2.5	2	2.5	2	2.25	3.81	1.8	Success
Inco 718	1.23	1.5	1.25	1.5	1.5	1.44	5.08	1.2	Underside Lip, Slight Negative Radius
Nim 75	1.23	6.5	6	6	6.5	6.25		5.1	43 mm Baseline Draw
Nim 75	1.23	2.75	2.75	2.5	2.5	2.63	2.54	2.1	Success
Nim 75	1.23	1.75	2	2	1.75	1.88	3.81	1.5	Success
Nim 75	1.23	Negative Radii all around part					5.08		Full Underside Lip & Negative Radius

Table 4 Calculated versus measured radius values

Mat'l	Mat'l Thickness (mm)	Edging Height (mm)	Calc r_1 (mm)	Calc r_1/t (mm)	Measured r_1 (mm)	Measured r_1/t	Radius Error	Absolute Rad Error, Ignoring Abnormalities	Abnormalities
C263	2.07				10.00	4.83			Baseline
C263	2.07	3.18	5.94	2.87	5.63	2.72	5%	5%	No
C263	2.07	5.08	3.50	1.69	3.50	1.69	0%	0%	No
C263	2.07	6.35	1.88	0.91	3.50	1.69	−46%		Yes
C263	2.07	8.89	−1.37	−0.66	3.75	1.81	−137%		Yes
Inco 718	1.23				6.88	5.59			Baseline
Inco 718	1.23	2.54	3.63	2.95	3.00	2.44	21%	21%	No
Inco 718	1.23	3.81	2.01	1.63	2.25	1.83	−11%	11%	No
Inco 718	1.23	5.08	0.38	0.31	1.44	1.17	−74%		Yes
Nim 75	1.23				6.25	5.08			Baseline
Nim 75	1.23	2.54	3.00	2.44	2.63	2.14	14%	14%	No
Nim 75	1.23	3.81	1.38	1.12	1.88	1.53	−27%	27%	No
Nim 75	1.23	5.1	−0.2	−0.2					Yes

Table 5 Percentage Error between calculated and measured baseline radius

Material	YS (MPa)	Calculated Radius (r_1, mm)	Measured Radius from baseline sample (r_1, mm)	Error
C263	385.3	10.06	10	0.58%
Inco 718	450.1	7.13	6.88	3.70%
Nim 75	482.4	7.65	6.25	22.34%

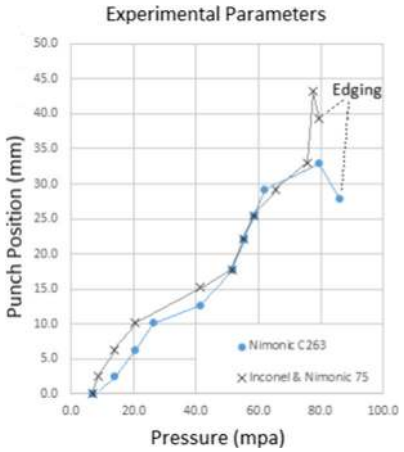

Fig. 24 Optimum forming parameters

Nimonic C263			Inconel 718 & Nimonic 75		
Punch Position (mm)	Bladder Pressure (MPa)	Dwell Time (sec)	Punch Position (mm)	Bladder Pressure (MPa)	Dwell Time (sec)
0.0	6.9	0	0.0	6.9	0
2.5	13.8	0	2.5	9.0	0
6.4	20.7	0	6.4	13.8	0
10.2	26.2	0	10.2	20.7	0
12.7	41.4	0	15.2	41.4	0
17.8	51.7	0	17.8	51.7	0
22.2	55.2	0	22.2	55.2	0
25.4	58.6	0	25.4	58.6	0
29.2	62.1	0	29.2	65.5	0
33.0	79.3	0	33.0	75.8	0
27.9	86.2	2	43.2	77.6	0
			39.4	79.3	2

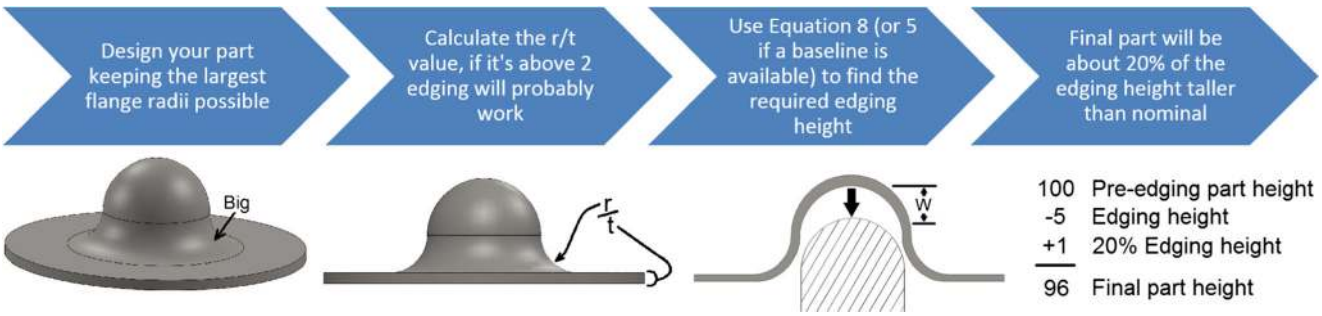

Fig. 25 Process design procedure for hydroforming with an edging operation

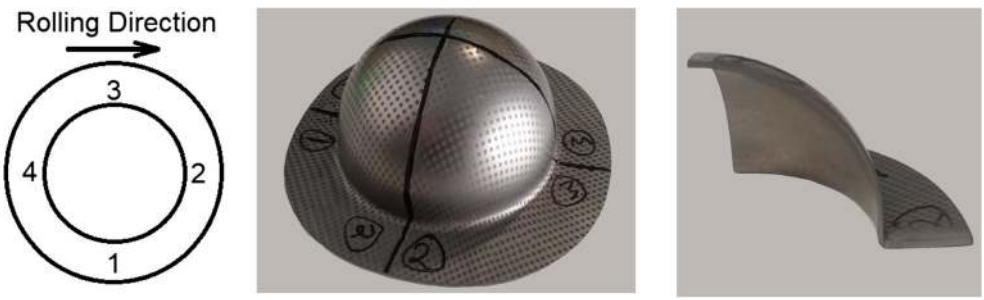

Fig. 26 Sections of test components used for thickness and radius measurements

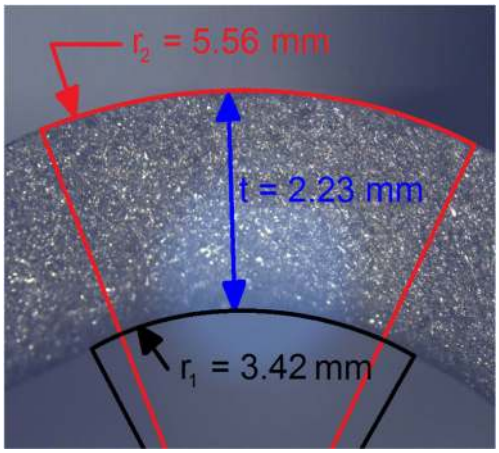

Fig. 27 Radius and thickness measurements C263 Zone 4

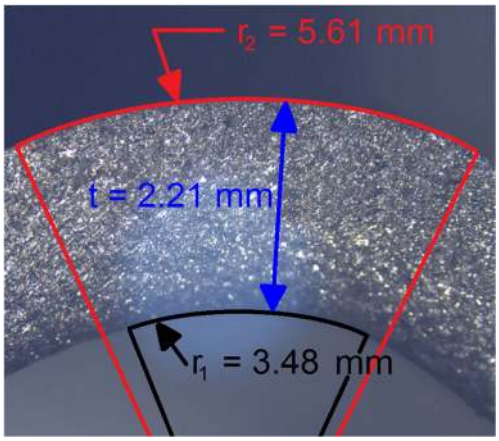

Fig. 28 Radius and thickness measurements C263 Zone 3

The radius measurements exhibited the highest standard deviation (0.16 mm) in the 4 measurements of the Inconel 718 sample. This means there is a small degree of additional uncertainty in the radius calculation (Eq. 5) which previously had an average error of ± 13% in this set of experiments. The thickness and deviation measurements are shown in Table 8.

Limitations & further work

Future work should focus on increasing the accuracy of the k coefficient with an increased sample size. The variation of k with different materials and possibly for different sizes should also be explored. So before use in industrial processes, trials should be performed to verify the values of coefficients with an appropriate degree of certainty (for different materials and thicknesses). Further work could also include a direct comparison of the effectiveness of coining and edging techniques. An investigation into the relationship between material thinning in the flange, draw depth and edging would be valuable, as would a study of non-edged versus edged radii thickness. Due to the limited material available for tensile tests, small samples were cut which were too small for an extensometer to be used. Consequently the strain hardening coefficient and anisotropy values could not be calculated which was unfortunate because these values would likely be useful to know and could possibly be worked into the equations generated to improve accuracy as these material properties have a large impact on the results of forming operations. Lastly, an experiment which uses a combination of process modelling (FEA) and physical trials to determine how accurate FEA can be during an edging operation and how to set one up properly, would be industrially useful.

Table 6 The effect of edging on overall part height

Mat'l	Final Punch Height (draw depth) as set on GUI (mm)	Measured Part Height (mm)	Amount of Edging Operation (mm)	Difference in Height as Compared to Baseline (mm)	Difference Between Edging Height and Part Height (mm)	r_1/t	Percentage Difference Between Edging Height & Part Height
C263	33.02	34.61				4.8	
C263	29.85	32.4	3.175	2.21	0.965	2.7	30.39%
C263	27.94	30.83	5.08	3.78	1.3	1.7	25.59%
C263	26.67	29.75	6.35	4.86	1.49	1.7	23.46%
C263	24.13	27.29	8.89	7.32	1.57	1.8	17.66%
Inco 718	43.18	44.07				5.6	
Inco 718	40.64	42.2	2.54	1.87	0.67	2.4	26.38%
Inco 718	39.37	40.85	3.81	3.22	0.59	1.8	15.49%
Inco 718	38.1	39.74	5.08	4.33	0.75	1.2	14.76%
Nim 75	43.18	44.21				5.1	
Nim 75	40.73	42.04	2.45	2.17	0.28	2.1	11.43%
Nim 75	39.37	40.82	3.81	3.39	0.42	1.5	11.02%
Nim 75	38.1	40.26	5.08	3.95	1.13		22.24%

Table 7 Comparison of optical and gauge radius measurements

Mat'l	Zone	Flange radius measured by radius gauge (mm)	Flange radius measured by microscopy (mm)	Difference (mm)	Absolute Percentage Difference
C263	1	3.5	3.43	0.07	2.00%
C263	2	3.5	3.42	0.08	2.29%
C263	3	3.5	3.48	0.02	0.57%
C263	4	3.5	3.58	−0.08	2.29%
Inco 718	1	2.5	2.56	−0.06	2.40%
Inco 718	2	2	2.46	−0.46	23.00%
Inco 718	3	2.5	2.50	0.00	0.00%
Inco 718	4	2	2.19	−0.19	9.50%
Nim 75	1	1.75	1.85	−0.10	5.71%
Nim 75	2	2	1.82	0.18	9.00%
Nim 75	3	2	1.92	0.08	4.00%
Nim 75	4	1.75	1.79	−0.04	2.29%

Conclusion

This paper presents the results of an experiment which investigated the effect of edging during a sheet hydroforming operation on three aerospace grade nickel alloys. The aim of this paper was to reduce the time taken by manufacturing engineers to develop an edging operation through the creation of a governing equation based upon an analytical model of the process. To this end an equation was derived that can be used to estimate a final radius in an edging operation. The main conclusions from this contribution can be briefly summarized as follows:

1. Edging is an effective technique which can significantly reduce a flange radius.
2. Excessive edging causes three separate types of phenomena, the first of which is crushing from the top, the second of which is curling the flange radius inwards creating a negative radius, and the third is the creation of a lip on the underside of the part.
3. Edging has a limitation in radius reduction. The sharpest radius that was achievable for the C263 alloy was 1.7 t (3.5 mm). The Inconel 718 and Nimonic 75 alloys were able to achieve a radius of 1.8 t and 1.5 t (2.25 & 1.875 mm) respectively.
4. Whn using a k value of 0.55, Eq. 5 calculates the radii found in the edging operations reasonably accurately with an average error of 13%. This equation becomes unstable with small r/t ratios of less than 2. The equation is not a definitive solution but gives an indication of a radius and is a good first step in an initial design. To be more definitive, the k value needs more testing. Especially important would be testing other materials for validation, or possibly the creation of alternate k values for different materials.
5. A decrease in punch height during an edging operation does not yield an identical decrease in overall part height. Generally, the reduction in part height is about 20% less than the reduction in punch height during an edging operation.
6. Material thickness in the radius is not significantly reduced by using the edging process, and in some instances actually increases.

This initial study has introduced the edging process and proposed a model to aid in the design of manufacturing operations. However there are several limitations to this work and further work is required to investigate a larger range of materials and create and validate numerical models of process behavior.

Table 8 Thickness, inside radius, & deviations

Mat'l	Zone	Thickness t (mm)	Radius r_1 (mm)	Radius r_2 (mm)	Ave t (mm)	σ t	Ave r_1 (mm)	σ r_1	Ave r_2 (mm)	σ r_2
C263	1	2.27	3.43	5.82	2.26	0.04	3.48	0.07	5.75	0.21
C263	2	2.31	3.42	5.56						
C263	3	2.21	3.48	5.60						
C263	4	2.23	3.58	6.02						
Inco 718	1	1.33	2.56	3.97	1.37	0.05	2.43	0.16	3.61	0.33
Inco 718	2	1.34	2.46	3.43						
Inco 718	3	1.36	2.50	3.79						
Inco 718	4	1.43	2.19	3.25						
Nim 75	1	1.41	1.85	2.56	1.43	0.04	1.85	.06	2.94	0.31
Nim 75	2	1.41	1.82	3.32						
Nim 75	3	1.39	1.92	2.89						
Nim 75	4	1.49	1.79	2.97						

Acknowledgments The authors would like to acknowledge support from the Engineering and Physical Science Research Council (EPSRC project EP/I015698/1), the Advanced Forming Research Centre, Rolls-Royce, and Triform for their continued funding and support of this work.

Funding This study was funded by Rolls-Royce and the EPSRC (project EP/I015698/1).

Compliance with ethical standards

Conflict of interest The authors declare that they have no conflict of interest.

References

1. Tolazzi M (2010) Hydroforming applications in automotive: a review. Int J Mater Form 3(S1):307–310
2. Bell C, Corney J, Savings D, Storr J (2015) Assessing the potential benefits of manufacturing gas turbine components by utilizing hydroforming technology. In 13th International Cold Forming Congress; 2nd - 4th September 2015, Glasgow
3. Zhang S, Wang Z, Xu Y, Wang Z, Zhou L (2004) Recent developments in sheet hydroforming technology. J Mater Process Technol 151(1-3):237–241
4. Bell C, Tamimi S, Corney J, Savings D (2016) Research directions in hydroforming technology. In AIP Conference Proceedings Vol. 1769. No. 1. AIP Publishing, Nantes
5. Koç M (2008) Hydroforming for advanced manufacturing, 1st edn. Woodhead Publishing Limited, Cambridge
6. GOM Optical Measuring Techniques (2009) Material properties: determination of process limitations in sheet metal forming - forming limit diagram. GOM Optical Measuring Techniques
7. Paul SK (2013) Theoretical analysis of strain-and stress-based forming limit diagrams. J Strain Anal Eng Des 48(3):177–188
8. Bell C, Jump E, Kerr W, Corney J, Zuelli N, Savings D (2017) Correlation between von Mises strain and material thinning in a hydroformed sample of Ti35A aerospace grade titanium. In AIP Conference Proceedings, vol. 1896, no. 1, p. 020029, Dublin
9. Herbertz R, Hermanns H, Labs R (2013) Massivumformung kurz und bündig. Deutsche Massivumformung. Hagen : Industrieverb. Massivumformung, Frankfurt
10. NeoNickel Alloy C263 Technical Data Sheet. [Online]. Available: https://www.neonickel.com/generate-alloy-pdf/?id=114. [Accessed 12 07 2018]
11. Special Metals Special Metals INCONEL Alloy 178. [Online]. Available: http://www.specialmetals.com/assets/smc/documents/inconel_alloy_718.pdf. [Accessed 12 7 2018]
12. Special Metals Special Metals. NIMONIC alloy 75. [Online]. Available: http://www.specialmetalswiggin.co.uk/pdfs/products/NIMONIC%20alloy%2075.pdf. [Accessed 12 7 2018]
13. Nakamura S, Sugiura H, Onoe H, Ikemoto K (1994) Hydromechanical drawing of automotive parts. J Mater Process Technol 46:431–503
14. Kobayashi S, Oh S-I, Altan T (1989) Metal forming and the finite-element method. Oxford University Press on Demand
15. Crapps J, Marin E, Horstemeyer M, Yassar R, Wang P (2010) Internal state variable plasticity-damage modeling of the copper tee-shaped tube hydroforming process. J Mater Process Technol 210(13):1726–1737, 2010
16. Ceretti E, Braga D, Giardini C (2010) Optimization of process parameters and part geometry for high diameter tube hydroforming. Int J Mater Form 3(S1):271–274
17. Danckert J, Nielsen KB (2000) Hydromechanical deep drawing with uniform pressure on the flange. CIRP Ann Manuf Technol 1(49):217–220
18. Wang H, Gao L, Chem M (2011) Hydrodynamic deep drawing process assisted by radial pressure with inward flowing liquid. Int J Mech Sci 53(9):793–799
19. Shang H, Qin S, Tay C (1997) Hydroforming sheet metal with intermittent changes in the draw-in condition of the flange. J Mater Process Technol 63(1–3):72–76
20. Aissa S, Mohamed S, Tarek L (2017) Experimental study of steam hydroforming of aluminum sheet metal. Exp Tech 41(5):525–533
21. Yuan S, Tang Z, Liu G (2013) Simulation and experiment on warm hydroforming of az31 magnesium alloy tube. In International Manufacturing Science and Engineering Conference collocated with the 41st North American Manufacturing Research Conference ASME
22. Landgrebe D, Schieck F (2015) Hot gas forming for advanced tubular automobile components: opportunities and challenges. In ASME 2015 International Manufacturing Science and Engineering Conference, Charlotte
23. Liu W, Xu Y, Yuan S (2014) Effect of pre-bulging on wrinkling of curved surface part by hydromechanical deep drawing. In 11th International Conference on Technology of Plasticity, Nagoya
24. Bach Fr-W, Kleiner M, Tekkaya AE (2013) Investigation of the Complex Interactions during Impulse Forming of Tubular Parts. Process Machine Interactions. Springer, Berlin, Heidelberg, 2013. 491–511.
25. Rösel S, Merklein M (2014) Improving formability due to an enhancement of sealing limits caused by using a smart fluid as active fluid medium for hydroforming. Production Engineering 8 1-2(8): 7–15
26. Wang Z-j, Xiang N, Wang P-y, Li Z-x (2017) Property-adjustable forming medium induced extension of sheet metal formability under variable magnetic field. J Mater Process Technol 243:420–432
27. Mohamed M, Carty D, Storr J, Zuelli N, Blackwell P, Savings D (2016) Feasibility study of complex sheet hydroforming process: experimental and Modelling. Key Eng Mater 716:685–691